

Zein/fucoidan-based composite nanoparticles for the encapsulation of pterostilbene: Preparation, characterization, physicochemical stability, and formation mechanism



Qianyuan Liu, Jingjing Chen, Yang Qin, Bo Jiang, Tao Zhang

PII: S0141-8130(20)32990-1

DOI: <https://doi.org/10.1016/j.ijbiomac.2020.04.128>

Reference: BIOMAC 15337

To appear in: *International Journal of Biological Macromolecules*

Received date: 5 November 2019

Revised date: 5 April 2020

Accepted date: 18 April 2020

Please cite this article as: Q. Liu, J. Chen, Y. Qin, et al., Zein/fucoidan-based composite nanoparticles for the encapsulation of pterostilbene: Preparation, characterization, physicochemical stability, and formation mechanism, *International Journal of Biological Macromolecules* (2020), <https://doi.org/10.1016/j.ijbiomac.2020.04.128>

This is a PDF file of an article that has undergone enhancements after acceptance, such as the addition of a cover page and metadata, and formatting for readability, but it is not yet the definitive version of record. This version will undergo additional copyediting, typesetting and review before it is published in its final form, but we are providing this version to give early visibility of the article. Please note that, during the production process, errors may be discovered which could affect the content, and all legal disclaimers that apply to the journal pertain.

Zein/fucoidan-based composite nanoparticles for the encapsulation of pterostilbene: preparation, characterization, physicochemical stability, and formation mechanism

Qianyuan Liu^{a,b}, Jingjing Chen^{a,b}, Yang Qin^{a,b}, Bo Jiang^{a,b,*}, Tao Zhang^{a,b}

^a State Key Laboratory of Food Science and Technology, Jiangnan University, Wuxi, Jiangsu, 214122, China

^b International Joint Laboratory on Food Safety, Jiangnan University, Wuxi, Jiangsu, 214122, China

***Corresponding author:** Bo Jiang

Tel: 86-510-85328307; Fax: 86-510-85913622

E-mail address: bjiang@jiangnan.edu.cn

Postal address: Jiangnan University, 1800 Lihu Avenue, Wuxi, Jiangsu, 214122, China

Abstract

The objective of this work is to fabricate zein/fucoidan composite nanoparticles for the delivery of pterostilbene, a hydrophobic nutraceutical with diverse beneficial biological activities. Pterostilbene-encapsulated zein/fucoidan composite nanoparticles were prepared using an anti-solvent precipitation method. The fucoidan levels affected the physicochemical properties of the composite nanoparticles. When the zein to fucoidan mass ratio was 10:1, 5:1, 2:1, or 1:1, the prepared zein/fucoidan nanoparticles were stable, and these nanoparticles showed higher pterostilbene encapsulation efficiency than did zein nanoparticles. Fucoidan-stabilized zein nanoparticles exhibited globular structure with average diameters of 120–150 nm. Fourier-transform infrared spectroscopy, X-ray diffraction, and fluorescence spectrum analysis confirmed that the formation of composite nanoparticles was mainly driven by electrostatic, hydrogen-bonding, and hydrophobic interactions between pterostilbene, zein, and fucoidan. Furthermore, the photochemical stability of pterostilbene encapsulated in zein/fucoidan nanoparticles was markedly better than that of pterostilbene loaded in zein nanoparticles or unencapsulated pterostilbene. Zein/fucoidan nanoparticles provided a better controlled release of pterostilbene than did zein nanoparticles under simulated gastrointestinal conditions. Moreover, the cytotoxicity assay demonstrated that zein/fucoidan nanoparticles were nontoxic to Caco-2, HK-2, and L-02 cells. Based on our results, the zein/fucoidan nanoparticles may be a promising delivery carrier for the encapsulation, protection, and release of pterostilbene.

Keywords: Pterostilbene; Zein/fucoidan composite nanoparticles; Formation mechanism

1. Introduction

Pterostilbene (PTS) (*trans*-3,5-dimethoxy-4-hydroxystilbene), a natural phenolic compound, is primarily present in many plants, especially in vaccinium berries and red sandalwood [1, 2]. Structurally, PTS is a dimethylether analog of resveratrol, a well-studied phenol, both of which are naturally bioactive compounds belonging to the stilbene family [1, 3]. PTS and resveratrol exhibit many similarly beneficial bioactivities, such as antioxidant, anti-inflammatory, anti-diabetic, and neuroprotective activities [4]. However, PTS has several advantages over resveratrol, such as a higher bioavailability and a greater metabolic stability, which is attributed to the fact that PTS possesses two methoxyl groups and one hydroxyl group while resveratrol contains three hydroxyl groups. The dimethylether structure of PTS can enhance its lipophilicity, causing a higher membrane permeability and cell absorption rate. Moreover, the methylation of the phenolic hydroxyl restricts the glucuronidation and sulfation of PTS due to less conjugating sites of hydroxyl groups, resulting in an improved metabolic stability [4]. Based on these chemical structural properties, PTS can be a promising compound as a nutraceutical, functional ingredient, or drug candidate in disease prevention and treatment.

However, native PTS exhibits a low aqueous solubility and a sensitivity to external agents such as air and light, which greatly limits its practical applications. For instance, PTS under ultraviolet irradiation can be converted into the *cis*-isomers, which are biologically less active than *trans*-isomers [5]. Recently, nanoencapsulation has been widely developed to overcome the aqueous solubility and stability issues of hydrophobic bioactive compounds, with numerous examples such as nanoemulsions [6], biopolymer nanoparticles [7], solid lipid nanoparticles [8], and liposomes [9]. Food-grade nanoparticle-based delivery vehicles applied to the encapsulation and delivery of hydrophobic bioactive compounds has attracted increasing attention. Food-grade carriers are usually fabricated using food-grade polymer materials, such as proteins and polysaccharides, which are generally biocompatible, biodegradable, and non-toxic [10]. Recently, zein-based nanoparticles have been widely used as carriers for the encapsulation of lipophilic bioactive compounds, such as β -carotene [11], curcumin [12], resveratrol [13], and quercetagenin [14]. Zein, a storage prolamin protein derived from maize, is rich in non-polar amino acids (e.g., leucine, alanine, and proline) and

also contains some polar amino-acid residues (e.g., glutamine), resulting in its high solubility in aqueous ethanol solution but low solubility in water alone [15, 16]. Due to its unique amphiphilic character, zein can easily self-assemble to form nanoparticles for the delivery of hydrophobic bioactive substances. However, zein colloidal nanoparticles are unstable under certain environmental conditions, such as pH values around the isoelectric point, elevated temperature, and high levels of salt. Previous research has shown that incorporation of anionic polysaccharides, such as hyaluronan [17], pectin [18], and carboxymethyl chitosan [19] can effectively improve the stability of zein nanoparticles through the formation of complexes, mainly based on interactions such as hydrogen bonds and electrostatic forces between zein and polysaccharides.

Fucoidan (FU), a sulfated anionic polysaccharide commonly extracted from marine brown algae and some echinoderms, mainly contains L-fucopyranose units and sulfated ester groups [20, 21]. The dissociation constant (pKa) value of sulfate groups on FU is around pH 2 [22]. At a pH value higher than the pKa of the polysaccharide but lower than the isoelectric point of zein (e.g., a pH between 2 to 6), FU is ionized with a negative charge, which has the potential to stabilize zein nanoparticles by interacting with cationic amino acid residues on the surface of zein nanoparticles, forming a negatively charged outer layer. Many previous researches have focused on the utilization of anionic polysaccharides containing carboxylate groups to stabilize zein nanoparticles. However, there are a few studies on the application of the polysaccharides possessing sulfated groups as stabilizers of zein nanoparticles. Cheng *et al.* [23] found that zein nanoparticles could be stabilized by ι -carrageenan, a kind of sulphated polysaccharide. In this case, ι -carrageenan-stabilized zein nanoparticles showed an excellent stability over a wide pH range. Yuan *et al.* [24] studied the use of dextran sulfate-coated zein nanoparticles as a vehicle for the delivery of curcumin. Nevertheless, to the best of our knowledge, there are no previous studies applying FU as a stabilizer of zein nanoparticles. To date, the study of biopolymer materials-stabilized zein nanoparticles as delivery systems for PTS has not been reported. Therefore, in the present work, we focus on the use of FU to form zein-biopolymer composite nanoparticles as a potential new carrier for PTS delivery.

In the current study, PTS was encapsulated into zein/FU composite nanoparticles using an anti-solvent precipitation method. The influence of the mass ratios of zein to FU on the

formation of zein/FU composite nanoparticles was explored. Factors including particle size, zeta-potential, PTS encapsulation efficiency, morphology, and physical stability of the PTS-loaded composite nanoparticles with different FU levels were characterized. In addition, the interaction mechanisms between PTS, zein, and FU were explored. The photochemical stability and *in vitro* release profiles of PTS in zein/FU composite nanoparticles were also investigated. Furthermore, the cytotoxicity of zein/FU composite nanoparticles was evaluated using Caco-2, HK-2, and L-02 cells. The composite nanoparticles developed in this work have a promising potential as delivery vehicles for PTS or hydrophobic nutraceuticals in the functional food and pharmaceutical industries. Moreover, the findings of present work may provide useful theoretical knowledge about the interaction between sulfated anionic polysaccharides and plant-derived proteins.

2. Materials and methods

2.1. Materials

Pterostilbene (purity 99%) was obtained from Great Forest Biomedical (Hangzhou, Zhejiang, China). Zein, fucoidan (extracted from *Fucus vesiculosus*), pepsin, and pancreatin were purchased from Sigma-Aldrich (St. Louis, MO, USA). Bile salts were purchased from Sangon Biotech (Shanghai, China). Other reagents, such as hydrochloric acid, sodium hydroxide, ethanol, acetonitrile, and ethyl acetate were of analytical grade and purchased from Sinopharm Chemical Reagent (Shanghai, China).

2.2. Preparation of zein/FU-PTS composite nanoparticles

PTS-zein/FU composite nanoparticles were fabricated using the anti-solvent precipitation method described in a previous report [25]. Briefly, zein (1%, w/v) and PTS (0.1%, w/v) were dissolved together in 75% (v/v) aqueous ethanol solution with stirring for 20 min. Different weighed amounts of FU (2.5, 5, 10, 20, 50, 100, and 200 mg) were added to 40 mL of water (adjusted to pH 3.5 by 1 M HCl) and stirred for 2 h to completely dissolve FU. Then, 10 mL zein-PTS aqueous ethanol solution was slowly added into 40 mL of FU solution with continuous stirring (1000 rpm) for 1 h to form PTS-zein/FU particle dispersions. Zein-PTS nanoparticle dispersions were prepared by adding the zein-PTS aqueous-ethanol solution into acid water (pH 3.5) as controls. Subsequently, ethanol in the dispersion was removed by a rotary evaporator, and the remaining nanoparticle dispersions were diluted with pH 3.5 water

to approximately 50 mL. Finally, the sample was centrifuged at 2000 *g* for 10 min to remove any possible large aggregates and undissolved substances. The final dispersions were stored at 4°C for the determination of various characteristics. A fraction of the dispersions was freeze-dried for further solid-state analysis.

The samples with different mass ratios of zein to FU at 100:2.5, 100:5, 100:10, 100:20, 100:50, 100:100, and 100:200 were denoted as PTS-zein/FU (40:1), PTS-zein/FU (20:1), PTS-zein/FU (10:1), PTS-zein/FU (5:1), PTS-zein/FU (2:1), PTS-zein/FU (1:1), and PTS-zein/FU (1: 2), respectively.

2.3. Particle size and zeta-potential

The effective mean particle size of the colloidal particles was determined by the dynamic light scattering technique (NanoBrook Omni Instrument, USA). The zeta-potential of colloidal particles was measured using a Zetasizer Nano ZS90 (Malvern Instruments Ltd., UK). Before measurements, the samples were diluted appropriately with pH 3.5 water to avoid multiple scattering effects.

2.4. Field emission scanning electron microscopy (FE-SEM)

The morphological structures of PTS-zein, PTS-zein/FU (10:1) PTS-zein/FU (2:1), and PTS-zein/FU (1:2) composite nanoparticles were observed by FE-SEM (Regulus 8100, Hitachi, Japan). A droplet of the freshly prepared colloidal particle dispersions was air-dried on the silicon chip, which was then adhered onto double-sided carbon tapes mounted to a specimen stub. Subsequently, the chips were coated with a thin gold layer and observed under 3.0 kV acceleration voltage.

2.5. Encapsulation efficiency (EE) and loading capacity (LC) of PTS

The EE and LC of the PTS loaded zein/FU nanoparticles were determined according to the report by Li *et al.* [26] with some modifications. Briefly, the freshly prepared nanoparticle dispersions were centrifuged at 2000 *g* for 10 min to remove any insoluble aggregates or free PTS. Then, 1 mL of particle dispersions were mixed with 1 mL of ethyl acetate and then the mixture was vortexed for 40 s. After phase separation, the upper organic phase was sucked out. The same extraction method was repeated for three times in order for the encapsulated PTS to fully dissolve into the upper organic phase (ethyl acetate). The upper organic phases were collected together, and then were properly diluted. The content of PTS dissolved in ethyl

acetate was measured using a HPLC system equipped with a C18 column at a detection wavelength of 305 nm. For the mobile phase, 55% (v/v) aqueous acetonitrile solution was used at a flow rate of 1 mL/min. The encapsulation efficiency (EE) and loading efficiency (LC) of PTS were calculated using the following equations:

$$EE (\%) = \frac{\text{weight of encapsulated PTS}}{\text{total weight of added PTS}} \times 100$$

$$LC (\%) = \frac{\text{weight of encapsulated PTS}}{\text{total weight of zein and FU input}} \times 100$$

2.6. Fluorescence spectroscopy

The fluorescence spectra of pure PTS, zein nanoparticles, PTS-zein nanoparticles, and PTS-zein/FU nanoparticles were measured using a fluorescence spectrophotometer (F-7000, Hitachi, Japan). The excitation wavelength was set at 280 nm and the emission signals were recorded from 290 to 440 nm. The scanning speed was 1200 nm/min. The slit widths of both the excitation and emission were fixed at 5 nm. The nanoparticle samples were diluted with pH 3.5 water at the same dilution ratios. Pure zein was dissolved in pure ethanol solution with an equivalent concentration as in the nanoparticle samples.

2.7. Fourier-transform infrared (FTIR) spectroscopy and X-ray diffraction (XRD)

The individual components (zein, FU, and PTS) and freeze-dried composite nanoparticle powders were measured by FTIR spectrophotometry (Nicolet iS10, Thermo Scientific Corporation, USA) and XRD (D2 PHASER, Bruker, Germany) according to a previous study [27]. The FTIR spectra were collected at wavenumbers ranging from 4000 to 400 cm^{-1} in 32 scans at a resolution of 4 cm^{-1} . The XRD data were acquired at a scanning angle (2θ) from 5° to 40° with a step size of 0.03° and a step time of 0.5 s. A copper (Cu) anode was used at a voltage of 30 kV and a current of 10 mA.

2.8. Stability evaluation

2.8.1. Physical stability

The physical stability of the PTS-zein/FU colloidal dispersions was determined using the LUMiSizer (LUM Corporation, Germany) by centrifugal force and light transmission. The samples were placed in LUM sample cells and centrifuged at a speed of 4000 rpm. The measurement wavelength was 870 nm. The first 100 profiles were obtained at an interval of 10 s, and the last 900 profiles were obtained at an interval of 60 s. The measurement

temperature was 25°C.

2.8.2. Photochemical stability

The photochemical stability against light-induced degradation of PTS was evaluated using a UV light lamp according to a report by Fan *et al.* [28]. Briefly, 2 mL of nanoparticle dispersions were added to a 6-well plate (25 cm² area), which was subjected to UV radiation at a wavelength of 254 nm for 15, 30, 45, 60, 90, and 120 min. Free PTS dissolved in acetonitrile was used as the control. The remaining PTS in the samples was analyzed using the HPLC procedure as described above.

2.9. *In vitro* release of PTS under simulated gastrointestinal conditions

The *in vitro* release profiles of PTS from the zein nanoparticles and zein/FU (2:1) nanoparticles were monitored under simulated gastric and intestinal conditions by using the dialysis method based on previous studies [29, 30] with some modifications. Briefly, simulated gastric fluid in a human eating state (SGF, pH 4.0 with 2.0 mg/mL NaCl and 3.2 mg/mL pepsin) and simulated intestinal fluid (SIF, pH 7.4 with 8.8 mg/mL NaCl, 6.8 mg/mL KH₂PO₄, 2 mg/mL pancreatin and 5 mg/mL bile salts) were prepared. Then, 3 mL of nanoparticle dispersions mixed with 3 mL of SGF were enclosed in a membrane dialysis bag (at 8-14 kDa molecular weight cut-off) and immersed in 60 mL of the SGF release medium for 2 h. Then, 6 mL of SIF was added to the dialysis bag, which was transferred to 120 mL of the SIF release medium for 4 h. The whole release process was carried out in an incubator at 37°C under continuous vibration at 120 rpm. At predetermined time points, aliquots (1 mL) of release medium were collected and replaced with 1 mL of fresh medium. The collected release medium was centrifuged at 10000 g for 10 min and the supernatant was passed through a 0.45 µm filter. Then, the amount of PTS released into the medium was measured using the HPLC method as described above.

2.10. Cytotoxicity assay

The cytotoxicity of the zein nanoparticles and zein/FU (2:1) nanoparticles was evaluated on Caco-2, HK-2, and L-02 cells using the CCK-8 assay (Beyotime Biotechnology, China) method according to a previous report with some modifications [31]. Briefly, the cells were seeded into 96-well culture plates at a cell density of 1×10^4 cells per well and placed in an incubator with 5% CO₂ at 37°C. After incubation for 24 h, the medium was removed and the

cells were treated with fresh medium containing various concentrations of composite nanoparticles (50, 100, 200, and 400 $\mu\text{g/mL}$, which corresponded to the concentrations of zein in the water phase). After 24 h of treatment, the sample media were removed and then culture medium containing 10% CCK-8 was added. After incubation for 2 h, the absorbance at 450 nm was measured using a microplate reader (Bio-Rad iMark, USA). The cell viability was calculated using the following equation:

$$\text{Cell viability (\%)} = \frac{\text{absorbances of treated cells}}{\text{absorbances of untreated cells}} \times 100$$

2.11. Statistical analysis

The results were reported as the mean \pm standard deviation of triplicate experimental results. The data were analyzed using SPSS software (IBM SPSS Statistics 21). The differences were evaluated using one-way analysis of variance (ANOVA) and Duncan's multiple comparisons. A result with a p -value below 0.05 ($p < 0.05$) was considered a statistically significant.

3. Results and discussion

3.1. Particle size and zeta-potential

The impact of the mass ratios of zein to FU on the mean particle diameter, particle size distribution, zeta-potential, and appearance of PTS-encapsulated zein/FU composite nanoparticles is shown in Fig. 1. In the absence of FU, PTS-loaded zein nanoparticles possessed a mean particle size of 73.77 nm, which is in agreement with a previous study that reported curcumin-enriched zein nanoparticles with a particle diameter of 77.29 nm [32]. The addition of FU to the anti-solvent aqueous phase was found to have a major impact on the mean particle diameter of composite nanoparticles, which varied with different mass ratios of zein to FU. As seen in Fig. 1D, when zein/FU mass ratio was 40:1 or 20:1, composite particle dispersions during the preparation were found to have markedly visual aggregation, gradually forming sediments at the bottom of the containers. This observation was representative of the generation of insoluble associative electrostatic complexes. These results might have been due to the formation of electrostatic attractions between zein and FU, leading the composite particles to carry a relatively low surface charge magnitude at the zein/FU mass ratios studied. Composite nanoparticles with a relatively low net surface charge showed a reduction in the

electrostatic repulsion between nanoparticles. This is one reason for the formation of insoluble electrostatic deposition around this FU level. This phenomenon can be further interpreted by the zeta-potential value of PTS-loaded zein/FU nanoparticles with different mass ratios of zein to FU (Fig. 1B). The zeta-potential of zein-PTS nanoparticles without the addition of FU was 49.63 mV at pH 3.5. The isoelectric point of zein is 6.2 [33], therefore zein has a positive charge at pH 3.5. FU contains sulfate ester groups which have been reported to have a pKa around pH 2.0 [22]. In an aqueous solution of pH 3.5, FU molecules carry a negative net charge. At a zein/FU mass ratio of 40:1, zein had a greater surface charge than FU, where the positive charge on the surface of the zein nanoparticles was only partially neutralized by the negative charge of FU molecule. Thus, due to the electrostatic attraction between zein and FU, the PTS-zein/FU (40:1) nanoparticles had a positive charge lower than zein-PTS nanoparticles. When the FU concentration increased, the FU molecule surface had a more negative charge, whereby the total net charge of the composite nanoparticles was negative. At a zein/FU mass ratio of 20:1, the levels of FU were insufficient to completely coat the surface of zein particles, which resulted in a single FU molecule coated on multiple zein nanoparticle surfaces, thus causing bridging flocculation. This could also be responsible for the aggregation of particles. A similar finding was reported by Li *et al.*, who found that when zein nanoparticles were mixed with soluble soybean polysaccharide at a mass ratio of 20:1 or 10:1, extensive particle aggregation occurred due to low electrostatic repulsion and bridging flocculation [34].

As the level of FU gradually increased (zein/FU mass ratio changing from 10:1 to 2:1), the particle size of PTS-loaded zein/FU nanoparticles was significantly ($p < 0.05$) decreased to 132.53 nm (zein/FU 10:1), 120.82 nm (zein/FU 5:1), and 117.59 nm (zein/FU 2:1). This result was ascribed to the fact that, as the FU content increased, the negative surface charge of the nanoparticles increased, leading to an increased electrostatic repulsion between the nanoparticles. Therefore, PTS-zein/FU nanoparticles formed a relatively compact structure, resulting in the reduction of particle size. As expected, the zeta-potential of the nanoparticles was decreased to -36.57 mV (zein/FU 10:1), -38.17 mV (zein/FU 5:1), and -38.03 mV (zein/FU 2:1) due to the increase in the electrostatic repulsion between the nanoparticles. Hu *et al.* reported that as alginate concentrations gradually increased to exceed the minimum

levels that could stabilize zein nanoparticles, the zeta-potential of the zein/alginate composite nanoparticles reached a relatively constant value [35]. Our results indicated that the FU was absorbed on the surface of zein nanoparticles by the attractive electrostatic interactions, and that negatively charged FU could stabilize the nanoparticles through electrostatic and steric repulsion.

Interestingly, as the amount of FU increased further (zein/FU ratio of 1:1 and 1:2), the mean size of the composite nanoparticles was significantly ($p < 0.05$) increased to 121.07 nm (zein/FU 1:1) and 139.32 nm (zein/FU 1:2). A similar phenomenon was observed by Chen *et al.* who pointed out that high levels of hyaluronic acid could increase the size of zein/hyaluronic acid nanoparticles due to cross-linking [36]. Our results suggested that the superfluous FU could produce cross-linking between nanoparticles. The zeta-potential of these nanoparticles showed no significant differences compared to the zein/FU (2:1) composite nanoparticles. These results further indicated the presence of anionic FU molecules coated on the surfaces of cationic zein particles, forming a core-shell nanoparticle with a zein core and a FU shell. Moreover, the FU shell layer dominated the overall charge of the composite nanoparticles.

3.2. FE-SEM analysis

The FE-SEM images of PTS-zein, PTS-zein/FU (10:1), PTS-zein/FU (2:1), and PTS-zein/FU (1:2) nanoparticles are presented in Fig. 2. PTS-zein nanoparticles (Fig. 2A) showed a spherical shape but with a coarse surface, probably owing to the presence of some PTS crystals at the surfaces of the zein nanoparticles [37]. Simultaneously, most particles were clumped and interconnected, and only a handful of individual particles could be clearly observed. This phenomenon is similar to that reported by Luo *et al.* [19], who used a similar method for the zein nanoparticles preparation. After the addition of FU, the composite nanoparticles exhibited smoother surfaces and a more regular spherical shape, which varied depending on the levels of FU. When the FU level was relatively low (zein/FU 10:1, Fig. 2B), the particles had a distinctly spherical shape but without a uniform size, which was ascribed to the fact that insufficient FU provided relatively weak interactions. In Fig. 2C, a relatively homogeneous size distribution and individual nanoparticles were observed in the PTS-zein/FU (2:1) nanoparticles, which was due to the strong interactions between zein, FU,

and PTS. At a zein/FU mass ratio of 1:2 (Fig. 2D), the nanoparticles connected with each other, which was attributed to excessive FU binding on the surface of the composite nanoparticles. The FE-SEM analysis was in accordance with the particle size results.

3.3. EE and LC of PTS

The EE and LC of PTS encapsulated in zein and zein/FU nanoparticles with different mass ratios of zein and FU are listed in Table 1. In the absence of FU, the EE of PTS enriched in zein nanoparticles was around 86.11%. At the zein to FU mass ratios of 40:1 and 20:1, the EE of the PTS in composite nanoparticles was significantly decreased to 47.27% and 27.63%, respectively. Since zein/FU (40:1) and zein/FU (20:1) samples tended to aggregate and precipitate during PTS encapsulation, which was due to a low electrostatic repulsion between the nanoparticles and bridging flocculation. Therefore, the LC of PTS in the zein/FU (40:1) and zein/FU (20:1) nanoparticles was markedly ($p < 0.05$) decreased compared to that of PTS in the zein nanoparticles. When the FU levels were increased from zein/FU (10:1) to zein/FU (1:2), the EE of the PTS in composite nanoparticles was significantly ($p < 0.05$) enhanced compared to that of the PTS in zein nanoparticles. In particular, the zein/FU (2:1) composite nanoparticles exhibited the highest EE of PTS, up to 95.63%. This finding indicated that the coating of zein nanoparticles with negatively charged FU could produce a nanoparticle with a compact structure, which could greatly improve the capacity of encapsulating PTS. The LC of PTS in the zein/FU (10:1) nanoparticles showed no significant difference compared to that of PTS in the zein nanoparticles. Furthermore, when the zein/FU mass ratio was increased from 5:1 to 1:1, the LC of the PTS in composite nanoparticles was found to be gradually reduced. These results were attributed to the fact that, as the FU concentration increased, the amount of encapsulated PTS in nanoparticles also increased slightly, however, the weight of the carriers was drastically improved. However, the EE and LC of PTS in zein/FU (1:2) nanoparticles were significantly decreased compared to that of PTS in the zein nanoparticles, which was due to the excessive levels of FU resulting in the formation of bridges with neighboring particles, promoting particle aggregation. These results suggested that incorporation of FU could effectively enhance the EE of PTS, resulting in that zein/FU composite nanoparticles could potentially be used as vehicles for the delivery of PTS.

3.4. Fluorescence spectroscopy

The fluorescence of the fluorophore is very sensitive to its surrounding micro-environment. The intermolecular interactions between proteins and other compounds may alter the local environment of proteins, which can be revealed through fluorescence spectroscopy [38]. Therefore, fluorescence spectrum measurements were performed to investigate the potential intermolecular interactions within nanoparticles.

The fluorescence emission spectra of pure zein, pure PTS, PTS-zein nanoparticle dispersions, and PTS-zein/FU nanoparticle dispersions are shown in Fig. 3. At an excitation wavelength of 280 nm, pure zein exhibited a fluorescence emission spectrum with a peak at 310 nm, which was attributed to the fact that zein contains a high level of tyrosine residues with a characteristic emission maximum around 304 nm. Interestingly, for pure PTS, a fluorescence emission peak at 388 nm was observed after being excited at 280 nm. When the PTS was encapsulated in composite nanoparticles, the typical fluorescence emission spectra of zein disappeared and was replaced by that of PTS. This phenomenon suggested that the presence of PTS could quench the intrinsic tyrosine fluorescence of zein, which can be explained by the growth of the PTS emission band excited by the transfer of energy and the molecular interactions. This result is similar to that reported by previous studies [39, 40]. Joye *et al.* reported that when resveratrol was mixed with gliadin, gliadin fluorescence spectra deviated from the tryptophan emission spectra and a new resveratrol emission band was observed, resulting from energy transfer and molecular interactions between gliadin and resveratrol [29]. Meanwhile, when PTS was loaded in zein and zein/FU nanoparticles, the PTS emission spectra showed a red shift to 395 nm and the fluorescence intensity considerably increased compared to pure PTS, which further indicated the existence of binding behavior and molecular interactions between PTS, zein and FU. After the addition of FU, the emission maximum peak of PTS did not undergo any changes, however, the fluorescence intensity was markedly decreased, compared to those of PTS-loaded zein nanoparticles. When the zein/FU mass ratios of 40:1, there was a relatively lower fluorescence intensity. The result was ascribed to the fact that there was a slight aggregation between nanoparticles when the low levels of FU were coated on the zein nanoparticles. As a result, the total quantity of PTS-zein/FU nanoparticles was reduced, resulting in a reduction in fluorescence intensity. At a zein/FU mass ratio of 20:1, there were many insoluble associative

electrostatic complexes at the bottom of the containers. The transparent upper dispersions contained very few composite particles formed by zein, FU, and PTS. Thus, the fluorescence spectrum of the PTS-zein/FU (20:1) nanoparticles was not determined. When the levels of FU were increased, the fluorescence emission intensity of PTS also increased; however, it remained lower than that of PTS in zein nanoparticles. This result was due to the fact that FU-coated zein nanoparticles were stable, and the addition of FU resulted in a more hydrophilic microenvironment for PTS, mainly driven by hydrophobic effects and hydrogen bonds. Wei *et al.* reported that the incorporation of rhamnolipid enhanced the polarity of the local environment of resveratrol, causing a decrease in the emission intensity of resveratrol [39].

3.5. Fourier-transform infrared (FTIR) spectroscopy

The FTIR spectra of the individual ingredients (pure zein, FU, and PTS) and composite nanoparticle samples are presented in Fig. 4. As shown in Fig. 4A, the spectrum of FU showed two characteristic absorption peaks at 1259.02 and 840.83 cm^{-1} , assigned to S=O stretching and C-O-S bending vibration, respectively, which were attributed to the existence of abundant sulfate ester groups in fucoidan [41, 42]. Two featured absorption peaks at 1654.49 and 1535.75 cm^{-1} were observed in the zein spectrum, which corresponded to amide I bands (C=O stretching) and amide II bands (C-N stretching and bending vibration of N-H groups), respectively [43]. The FTIR spectrum of PTS exhibited characteristic absorption bands at 1600.15, 1585.55, 1514.71, 1458.43, 1353.35, and 963.31 cm^{-1} , assigned to aromatic -C=C- stretching, olefinic -C=C- stretching, aromatic ring -C=C- stretching, aromatic ring -C=C- stretching, -C-O- stretching vibration, and trans olefinic -C=C- stretching, respectively [39]. Furthermore, the pure FU, zein, and PTS also exhibited prominent absorption peaks at 3440, 3390, and 3310 cm^{-1} , respectively, which were associated with O-H stretching vibrations.

The FTIR spectra of the PTS-zein/FU nanoparticles at different mass ratios of zein to FU were also evaluated (Fig. 4B). As the FU levels were gradually increased, the absorption band of O-H vibration at 3500–3100 cm^{-1} was shifted to 3304.23 cm^{-1} (PTS-zein), 3304.84 cm^{-1} (PTS-zein/FU 40:1), 3312.51 cm^{-1} (PTS-zein/FU 20:1), 3304.73 cm^{-1} (PTS-zein/FU 10:1), 3308.71 cm^{-1} (PTS-zein/FU 5:1), 3323.58 cm^{-1} (PTS-zein/FU 2:1), 3432.53 cm^{-1}

(PTS-zein/FU 1:1), and 3440.52 cm^{-1} (PTS-zein/FU 1:2). These findings demonstrated that hydrogen bonding may be generated between zein, FU, and PTS [44]. Additionally, in comparison with the spectrum of pure zein, the amide II peaks in the PTS-zein/FU composite nanoparticles shifted from 1535.75 cm^{-1} to 1540.66 , 1540.20 , 1540.98 , 1539.01 , 1540.45 , 1539.86 , 1541.08 , and 1540.47 cm^{-1} , at the zein to FU mass ratios of 40:1, 20:1, 10:1, 5:1, 2:1, 1:1, and 1:2, respectively. These results suggested that electrostatic interactions may be formed between zein, FU, and PTS during the production of composite nanoparticles [39]. Interestingly, when PTS was incorporated into the nanoparticles, the featured absorption bands observed in the spectrum of pure PTS disappeared, which indicated that the characteristic peaks of PTS merged or overlapped with the absorption bands of the polymer matrix, suggesting that PTS was embedded in the composite nanoparticles. These findings suggested that hydrogen-bonding, hydrophobic effects, and electrostatic attraction were the main mechanisms involved in the production of PTS-zein/FU composite nanoparticles.

3.6. X-ray diffraction (XRD)

The XRD spectra of pure PTS, pure zein, pure FU, and composite nanoparticles are shown in Fig. 5. The XRD pattern of zein showed two wide humps at diffraction angles 2θ of 9.0° and 19.6° , while FU exhibited one broad peak, which indicated the amorphous nature of zein and FU. Conversely, pure PTS powder exhibited sharp diffraction peaks (2θ) mainly at 8.4° , 12.5° , 17.9° , 18.5° , 23.1° , 25.3° , and 28.1° , which demonstrated the highly crystallized form of pure PTS. After PTS was encapsulated into the composite nanoparticles, the sharp characteristic crystalline peaks of pure PTS were not observed in any of the composite nanoparticles, indicating that the state of PTS changed from crystallinity to amorphous form, thus providing a convincing evidence of encapsulation. Additionally, the peak intensities of the zein/FU composite nanoparticles at 9.0° and 19.6° diffraction angles were both markedly decreased in comparison with native zein molecules. Interestingly, two characteristic new peaks around 28° and 31° were found in the spectra of the PTS-loaded zein/FU nanoparticles, which may be due to the intermolecular interactions between zein, FU, and PTS.

3.7. Physical stability

LUMiSizer can be used to obtain a transmission fingerprint of the dispersion system to define the characteristics of the system, such as stability, phase separation behavior (such as

creaming and sedimentation), and particle interaction (such as flocculation and coalescence). The transmission fingerprints of the zein/FU composite nanoparticles at different mass ratios of zein to FU were monitored during centrifugation (Fig. S1). The transmission profile showed space-related and time-related transmission changes over the entire sample length, which can trace the demixing behavior and characterize the stability of the samples. After the nanoparticle dispersions were centrifuged, the particles became unstable. Then, the light transmission intensity was found to gradually increase at the top of the sample cell, indicating the occurrence of destabilization phenomena, including sedimentation, flocculation, or creaming. As shown in Fig. S1, the different nanoparticles showed similar phase separation progress, although to different degrees. The change rate of transmission can reflect the instability of the samples (Fig. S2). The instability index of the different nanoparticles is summarized in Fig. 6.

At a zein/FU mass ratio of 20:1, the particles were obviously sedimented at the bottom, leading to transparent upper dispersions. Thus, it was unnecessary to test the transmission change. In the Fig. 6, PTS-zein/FU (40:1) nanoparticles showed the highest instability index, indicating a lower stability than other nanoparticle samples. This result may be due to low electrostatic repulsion between the nanoparticles and bridging flocculation when the amount of FU added was insufficient. As the concentration of FU was increased (zein/FU mass ratios of 10:1, 5:1, and 2:1), the instability index of was decreased, namely, physical stability of nanoparticle dispersions was increased. In particular, PTS-zein/FU (2:1) nanoparticles showed the highest physical stability. The increase in FU levels resulted in the increase of the negative charge of composite nanoparticles, which could provide enough electrostatic repulsion to form a relatively compact nanoparticle structure. When zein to FU mass ratio was 1:1 or 2:1, the instability index of composite nanoparticles was increased, which suggested that excessive FU might weaken the physical stability of nanoparticles. Cross-linking by excessive FU may have led to a decrease in steric stability. This result is consistent with a previous study pointing out that excessive rhamnolipids decreased the physical stability of zein-PGA-rhamnolipid nanoparticles due to the bridging effect [45]. Our stability results were in perfect agreement with the particle size and zeta-potential analyses presented in this study.

3.8. Photochemical stability

The photochemical stability of PTS loaded in zein and zein/FU nanoparticles compared with free PTS is shown in Fig. 7. The retention of PTS was decreased as the UV irradiation time increased. This result was attributed to the stilbene structure of PTS, which absorbs UV light, resulting in its degradation and isomerization when subjected to UV irradiation [29, 46]. During UV light treatment, the PTS-loaded composite nanoparticles were relatively more stable than free PTS. The retention rates of PTS in zein nanoparticles and zein/FU nanoparticles were higher than those of free PTS after UV irradiation. In addition, the PTS retention rates in the zein/FU nanoparticles were higher than in the zein nanoparticles. For example, after exposure to UV light for 90 min and 120 min, PTS was almost completely degraded, and the retention of PTS was not detected by HPLC after UV irradiation for 120 min. Meanwhile, the retention rates of PTS increased to 11.0% and 13.9% when loaded in the zein and zein/FU nanoparticles, respectively. The nanoparticles were able to protect PTS from degradation, which could be explained by the fact that zein molecules contain aromatic amino acid residues and double bonds capable of absorbing some of the UV light [47]. Regarding the zein/FU nanoparticles, FU might coat the surface of the composite nanoparticles to form an outer layer, which could provide a physical barrier to protect PTS from UV light, increasing the photochemical stability of PTS. In a previous study, Sun *et al.* reported that a polymer matrix comprised of zein/shellac nanoparticles provided curcumin with protection from UV irradiation [48].

3.9. *In vitro* release of PTS

The *in vitro* release profiles of PTS from zein nanoparticles and zein/FU nanoparticles in simulated gastric fluid for the eating state and under simulated intestinal fluid conditions were investigated. The stomach digestive juice in a human eating state was chosen for simulation since most oral medications are taken after meals [29]. As shown in Fig. 8, PTS-zein nanoparticles and PTS-zein/FU (2:1) nanoparticles exhibited a similar PTS release profile in SGF medium. After 120 min of gastric digestion, the accumulated amount of PTS released from PTS-zein nanoparticles and PTS-zein/FU (2:1) nanoparticles was 19% and 21%, respectively. When samples from the SGF digestion were transferred to the SIF stage, we observed a fast release in the initial 60 min of the SIF digestion stage (120-180 min), followed by a sustained release for up to 360 min. This rapid release result may be due to the existence

of bile salts, proteins, and peptides in the simulated intestinal juices, which could form mixed micelles or complexes to solubilize the released PTS [49]. At the end of the small intestinal digestion, the cumulative release of PTS from zein/FU nanoparticles was 46%, which was significantly lower than that from zein nanoparticles (58%). A slightly slower PTS release in the SGF medium was attributed to the fact that the FU was absorbed on the surface of zein, which may have provided a barrier against PTS release [50]. In addition, the PTS-zein/FU (2:1) nanoparticles had a more compact structure due to the strong interactions between zein, FU, and PTS, which could inhibit PTS release from nanoparticles [39]. These results demonstrated that FU-stabilized zein nanoparticles could effectively reduce the release of PTS and achieved a controlled release under simulated gastrointestinal conditions. The release results are similar to those presented in the study by Wang *et al.*, who reported that that carboxymethyl chitosan and tea polyphenols coated on zein nanoparticles reduced the release rate of encapsulated β -carotene, since the coatings could form a dense coating layers to greatly protect zein from digestive degradation and provide a good barrier against β -carotene release [11]. Overall, the zein/FU composite nanoparticles have great potential to be applied as an oral delivery vehicle for PTS or other hydrophobic nutrients.

3.10. Cytotoxicity assay

The cell viability of Caco-2, HK-2, and L-02 cells treated with zein and zein/FU (2:1) composite nanoparticles for 24 h was tested as shown in Fig. 9. After 24 h of treatment with composite nanoparticles at a concentration of 400 $\mu\text{g}/\text{mL}$, the cell viability was 94.2%, 94.8%, and 96.3% for Caco-2, HK-2, and L-02 cells, respectively. Compared with the control group, the zein and zein/FU (2:1) nanoparticles did not have a significant ($p > 0.05$) toxic effect on the cell viability of Caco-2, HK-2, and L-02 cells at any concentrations (50, 100, 200, and 400 $\mu\text{g}/\text{mL}$). These results indicated that these nanoparticles were nontoxic and biocompatible at such used concentrations, which may be due to the fact that the natural biopolymers were used as carrier materials. Therefore, the zein/FU composite nanoparticles fabricated in this study can be used as a safe carrier for the delivery of pterostilbene or other lipophilic nutrients.

3.11. Formation mechanism of composite nanoparticles

The formation mechanism of zein/FU composite nanoparticles is proposed in a

schematic illustration (Fig. 10). In brief, zein and PTS co-dissolved in 75% aqueous ethanol solution were dropwise added into anti-solvents (pH 3.5 water containing FU) with magnetic stirring. Subsequently, the ethanol in the dispersions was completely removed by vacuum evaporation. Due to the decrease in the ethanol concentration, the solubility of zein was reduced, thus resulting in zein precipitate and self-assemble into composite nanoparticles with FU and PTS. The formation of PTS-zein/FU composite nanoparticles was primarily driven by hydrogen bonds, electrostatic interactions, and hydrophobic effects between zein, FU, and PTS, which was demonstrated via fluorescence spectrum, FTIR, and XRD analysis. Moreover, based on the results of particle size and zeta-potential, the formation process of PTS-loaded zein/FU composite nanoparticles was influenced by variations in the levels of FU. At zein/FU mass ratio of 40:1 or 20:1, the FU molecule was insufficient to fully coat the zein nanoparticles surfaces, leading to a bridging flocculation and a low electrostatic repulsion, resulting in the aggregation of particles and a relatively low net magnitude. At higher FU levels (zein/FU mass ratio of 10:1, 5:1, or 2:1), the particle surfaces were completely coated with the negatively charged FU molecules. Here, as the FU levels increased, the interactions between zein, FU, and PTS were enhanced, resulting in the formation of compact and stable composite nanoparticles with smaller particle size. As FU levels further increased (zein/FU mass ratio of 1:1 or 2:1), an excess of FU resulted in cross-linking, causing an increase in particle size. These formation mechanisms were strongly confirmed by the physical stability and the FE-SEM observation of composite nanoparticles at different zein/FU mass ratios. Furthermore, the PTS in the zein/FU (1:2) nanoparticles showed a higher encapsulation efficiency and a better photochemical stability than PTS in zein nanoparticles alone.

In conclusion, our results indicate that zein/FU composite nanoparticles have the potential to be used as all-natural delivery systems for PTS or other lipophilic bioactive compounds. Moreover, our findings may provide some information about interaction between zein and FU.

CRedit authorship contribution statement

Qianyuan Liu: Conceptualization, Methodology, Software, Writing - original draft, Data curation. **Jingjing Chen:** Formal analysis, Investigation. **Yang Qin:** Software. **Tao Zhang:** Formal analysis, Investigation. **Bo Jiang:** Project administration, Funding acquisition,

Writing - review & editing.

Funding

This research was supported by the National Key Research and Development Program of China (No. 2017YFC1600902), the National Natural Science Foundation of China (No. 31871745 and No. 21702076), and the National First-Class Discipline Program of Food Science and Technology (No. JUFSTR20180203).

Declaration of competing interest

The authors declare no conflict of interests associated with this publication.

References

- [1] R.M. Peng, G.R. Lin, Y. Ting, J.Y. Hu, Oral delivery system enhanced the bioavailability of stilbenes: Resveratrol and pterostilbene, *BioFactors* 44 (1) (2018) 5-15.
- [2] A.M. Rimando, W. Kalt, J.B. Magee, J. Dewey, J.R. Ballington, Resveratrol, Pterostilbene, and Piceatannol in Vaccinium Berries, *Journal of Agricultural and Food Chemistry* 52 (15) (2004) 4713-4719.
- [3] K.W. Lange, S. Li, Resveratrol, pterostilbene, and dementia, *BioFactors* 44 (1) (2018) 83-90.
- [4] P. Wang, S. Sang, Metabolism and pharmacokinetics of resveratrol and pterostilbene, *BioFactors* 44 (1) (2018) 16-25.
- [5] F. Silva, A. Figueiras, E. Gallardo, C. Nerín, F.C. Domingues, Strategies to improve the solubility and stability of stilbene antioxidants: A comparative study between cyclodextrins and bile acids, *Food Chemistry* 145 (2014) 115-125.
- [6] J. Chen, F. Li, Z. Li, D.J. McClements, H. Xiao, Encapsulation of carotenoids in emulsion-based delivery systems: Enhancement of β -carotene water-dispersibility and chemical stability, *Food Hydrocolloids* 69 (2017) 49-55.
- [7] C. Chang, T. Wang, Q. Hu, Y. Luo, Zein/caseinate/pectin complex nanoparticles: Formation and characterization, *International Journal of Biological Macromolecules* 104 (2017) 117-124.
- [8] T. Wang, Q. Hu, J.Y. Lee, Y. Luo, Solid Lipid-Polymer Hybrid Nanoparticles by In Situ Conjugation for Oral Delivery of Astaxanthin, *Journal of Agricultural and Food Chemistry* 66 (36) (2018) 9473-9480.
- [9] A. Courtois, M. Garcia, S. Krisa, C. Atgié, P. Sauviant, T. Richard, C. Faure, Encapsulation of ϵ -viniferin in onion-type multi-lamellar liposomes increases its solubility and its photo-stability and decreases its cytotoxicity on Caco-2 intestinal cells, *Food & Function* 10 (5) (2019) 2573-2582.
- [10] J.J. Iris, D.J. McClements, Biopolymer-Based Delivery Systems: Challenges and Opportunities, *Current Topics in Medicinal Chemistry* 16 (9) (2016) 1026-1039.
- [11] M. Wang, Y. Fu, G. Chen, Y. Shi, X. Li, H. Zhang, Y. Shen, Fabrication and characterization of carboxymethyl chitosan and tea polyphenols coating on zein nanoparticles to encapsulate β -carotene by anti-solvent precipitation method, *Food Hydrocolloids* 77 (2018) 577-587.
- [12] M.F. Li, L. Chen, M.Z. Xu, J.L. Zhang, Q. Wang, Q.Z. Zeng, X.C. Wei, Y. Yuan, The formation of zein-chitosan complex coacervated particles: Relationship to encapsulation and controlled release properties, *International Journal of Biological Macromolecules* 116 (2018) 1232-1239.
- [13] R. Penalva, I. Esparza, E. Larraneta, C.J. González-Navarro, C. Gamazo, J.M. Irache, Zein-Based

Nanoparticles Improve the Oral Bioavailability of Resveratrol and Its Anti-inflammatory Effects in a Mouse Model of Endotoxic Shock, *Journal of Agricultural and Food Chemistry* 63 (23) (2015) 5603-5611.

[14] C. Sun, L. Dai, Y. Gao, Binary Complex Based on Zein and Propylene Glycol Alginate for Delivery of Quercetagenin, *Biomacromolecules* 17 (12) (2016) 3973-3985.

[15] M.R. Kasaai, Zein and zein -based nano-materials for food and nutrition applications: A review, *Trends in Food Science & Technology* 79 (2018) 184-197.

[16] J.A. Tapia-Hernández, F. Rodríguez-Felix, J.E. Juárez-Onofre, S. Ruiz-Cruz, M.A. Robles-García, J. Borboa-Flores, F.J. Wong-Corral, F.J. Cinco-Moroyoqui, D.D. Castro-Enríquez, C.L. Del-Toro-Sánchez, Zein-polysaccharide nanoparticles as matrices for antioxidant compounds: A strategy for prevention of chronic degenerative diseases, *Food Research International* 111 (2018) 451-471.

[17] S. Chen, Y. Han, C. Sun, L. Dai, S. Yang, Y. Wei, L. Mao, F. Yuan, Y. Gao, Effect of molecular weight of hyaluronan on zein-based nanoparticles: Fabrication, structural characterization and delivery of curcumin, *Carbohydrate Polymers* 201 (2018) 599-607.

[18] Y. Jiang, C. Zhang, J. Yuan, Y. Wu, F. Li, D. Li, Q. Huang, Effects of pectin polydispersity on zein/pectin composite nanoparticles (ZAPs) as high internal-phase Pickering emulsion stabilizers, *Carbohydrate Polymers* 219 (2019) 77-86.

[19] Y. Luo, Z. Teng, Q. Wang, Development of Zein Nanoparticles Coated with Carboxymethyl Chitosan for Encapsulation and Controlled Release of Vitamin D3, *Journal of Agricultural and Food Chemistry* 60 (3) (2012) 836-843.

[20] K.Y. Lu, R. Li, C.H. Hsu, C.W. Lin, S.C. Chou, M.L. Tsai, F.L. Mi, Development of a new type of multifunctional fucoidan-based nanoparticles for anticancer drug delivery, *Carbohydrate Polymers* 165 (2017) 410-420.

[21] L. Cunha, A. Grenha, Sulfated Seaweed Polysaccharides as Multifunctional Materials in Drug Delivery Applications, *Marine Drugs* 14 (3) (2016) 42.

[22] Y.S. Gu, E.A. Decker, D.J. McClements, Influence of pH and carrageenan type on properties of β -lactoglobulin stabilized oil-in-water emulsions, *Food Hydrocolloids* 19 (1) (2005) 83-91.

[23] C.J. Cheng, O.G. Jones, Stabilizing zein nanoparticle dispersions with ι -carrageenan, *Food Hydrocolloids* 69 (2017) 28-35.

[24] Y. Yuan, H. Li, J. Zhu, C. Liu, X. Sun, D. Wang, Y. Xu, Fabrication and characterization of zein nanoparticles by dextran sulfate coating as vehicles for delivery of curcumin, *International Journal of Biological Macromolecules* (2019) (10.1016/j.ijbiomac.2019.10.149).

[25] J. Chen, J. Zheng, E.A. Decker, D.J. McClements, H. Xiao, Improving nutraceutical bioavailability using mixed colloidal delivery systems: lipid nanoparticles increase tangeretin bioaccessibility and absorption from tangeretin-loaded zein nanoparticles, *RSC Advances* 5 (90) (2015) 73892-73900.

[26] H. Li, Y. Xu, X. Sun, S. Wang, J. Wang, J. Zhu, D. Wang, L. Zhao, Stability, bioactivity, and bioaccessibility of fucoxanthin in zein-caseinate composite nanoparticles fabricated at neutral pH by antisolvent precipitation, *Food Hydrocolloids* 84 (2018) 379-388.

[27] J. Liang, H. Yan, X. Wang, Y. Zhou, X. Gao, P. Puligundla, X. Wan, Encapsulation of epigallocatechin gallate in zein/chitosan nanoparticles for controlled applications in food systems, *Food Chemistry* 231 (2017) 19-24.

[28] Y. Fan, Y. Liu, L. Gao, Y. Zhang, J. Yi, Improved chemical stability and cellular antioxidant

activity of resveratrol in zein nanoparticle with bovine serum albumin-caffeic acid conjugate, *Food Chemistry* 261 (2018) 283-291.

[29] Q. Liu, Y. Jing, C. Han, H. Zhang, Y. Tian, Encapsulation of curcumin in zein/ caseinate/sodium alginate nanoparticles with improved physicochemical and controlled release properties, *Food Hydrocolloids* 93 (2019) 432-442.

[30] S. Chen, Y. Han, Y. Wang, X. Yang, C. Sun, L. Mao, Y. Gao, Zein-hyaluronic acid binary complex as a delivery vehicle of quercetagenin: Fabrication, structural characterization, physicochemical stability and in vitro release property, *Food Chemistry* 276 (2019) 322-332.

[31] G. Heep, A. Almeida, R. Marcano, D. Vieira, R.M. Mainardes, N.M. Khalil, B. Sarmento, Zein-casein-lysine multicomposite nanoparticles are effective in modulate the intestinal permeability of ferulic acid, *International Journal of Biological Macromolecules* 138 (2019) 244-251.

[32] L. Dai, R. Li, Y. Wei, C. Sun, L. Mao, Y. Gao, Fabrication of zein and rhamnolipid complex nanoparticles to enhance the stability and in vitro release of curcumin, *Food Hydrocolloids* 77 (2018) 617-628.

[33] R. Shukla, M. Cheryan, Zein: the industrial protein from corn, *Industrial Crops and Products* 13 (3) (2001) 171-192.

[34] H. Li, D. Wang, C. Liu, J. Zhu, M. Fan, X. Sun, T. Wang, Y. Xu, Y. Cao, Fabrication of stable zein nanoparticles coated with soluble soybean polysaccharide for encapsulation of quercetin, *Food Hydrocolloids* 87 (2019) 342-351.

[35] K. Hu, D.J. McClements, Fabrication of biopolymer nanoparticles by antisolvent precipitation and electrostatic deposition: Zein-alginate core/shell nanoparticles, *Food Hydrocolloids* 44 (2015) 101-108.

[36] S. Chen, C. Sun, Y. Wang, Y. Han, L. Dai, A. Abliz, Y. Gao, Quercetagenin-Loaded Composite Nanoparticles Based on Zein and Hyaluronic Acid: Formation, Characterization, and Physicochemical Stability, *Journal of Agricultural and Food Chemistry* 66 (28) (2018) 7441-7450.

[37] L. Dai, Y. Wei, C. Sun, L. Mao, D.J. McClements, Y. Gao, Development of protein-polysaccharide-surfactant ternary complex particles as delivery vehicles for curcumin, *Food Hydrocolloids* 85 (2018) 75-85.

[38] P. Kaushik, K. Rawat, V.K. Aswal, J. Kohlbrecher, H.B. Bohidar, Fluorescent complex coacervates of agar and in situ formed zein nanoparticles: Role of electrostatic forces, *Carbohydrate Polymers* 224 (2019) 115150.

[39] Y. Wei, Z. Yu, K. Lin, C. Sun, L. Dai, S. Yang, L. Mao, F. Yuan, Y. Gao, Fabrication and characterization of resveratrol loaded zein-propylene glycol alginate-rhamnolipid composite nanoparticles: Physicochemical stability, formation mechanism and in vitro digestion, *Food Hydrocolloids* 95 (2019) 336-348.

[40] I.J. Joye, G. Davidov-Pardo, R.D. Ludescher, D.J. McClements, Fluorescence quenching study of resveratrol binding to zein and gliadin: Towards a more rational approach to resveratrol encapsulation using water-insoluble proteins, *Food Chemistry* 185 (2015) 261-267.

[41] C.H. Chen, Y.S. Lin, S.J. Wu, F.L. Mi, Multifunctional nanoparticles prepared from arginine-modified chitosan and thiolated fucoidan for oral delivery of hydrophobic and hydrophilic drugs, *Carbohydrate Polymers* 193 (2018) 163-172.

[42] L.C. Tsai, C.H. Chen, C.W. Lin, Y.C. Ho, F.L. Mi, Development of multifunctional nanoparticles self-assembled from trimethyl chitosan and fucoidan for enhanced oral delivery of insulin, *International Journal of Biological Macromolecules* 126 (2019) 141-150.

[43] L. Dai, C. Sun, Y. Wei, X. Zhan, L. Mao, Y. Gao, Formation and characterization of

zein-propylene glycol alginate-surfactant ternary complexes: Effect of surfactant type, *Food Chemistry* 258 (2018) 321-330.

[44] C. Sun, L. Dai, Y. Gao, Formation and characterization of the binary complex between zein and propylene glycol alginate at neutral pH, *Food Hydrocolloids* 64 (2017) 36-47.

[45] F. Zhang, M.A. Khan, H. Cheng, L. Liang, Co-encapsulation of α -tocopherol and resveratrol within zein nanoparticles: Impact on antioxidant activity and stability, *Journal of Food Engineering* 247 (2019) 9-18.

[46] B.C. Trela, A.L. Waterhouse, Resveratrol: Isomeric Molar Absorptivities and Stability, *Journal of Agricultural and Food Chemistry* 44 (5) (1996) 1253-1257.

[47] L. Dai, C. Sun, R. Li, L. Mao, F. Liu, Y. Gao, Structural characterization, formation mechanism and stability of curcumin in zein-lecithin composite nanoparticles fabricated by antisolvent co-precipitation, *Food Chemistry* 237 (2017) 1163-1171.

[48] C. Sun, C. Xu, L. Mao, D. Wang, J. Yang, Y. Gao, Preparation, characterization and stability of curcumin-loaded zein-shellac composite colloidal particles, *Food Chemistry* 228 (2017) 656-667.

[49] X. Huang, Y. Liu, Y. Zou, X. Liang, Y. Peng, D.J. McClements, K. Hu, Encapsulation of resveratrol in zein/pectin core-shell nanoparticles: Stability, bioaccessibility, and antioxidant capacity after simulated gastrointestinal digestion, *Food Hydrocolloids* 93 (2019) 261-269.

[50] M.A. Khan, C. Yue, Z. Fang, S. Hu, H. Cheng, A.M. Bakry, L. Liang, Alginate/chitosan-coated zein nanoparticles for the delivery of resveratrol, *Journal of Food Engineering* 258 (2019) 45-53.

Figure captions

Fig. 1. Mean particle size (A), zeta-potential (B), and particle size distribution (C) of PTS-zein nanoparticles and PTS-zein/FU composite nanoparticles with different mass ratios of zein to FU. The photograph (D) showed the appearance of prepared dispersions. The different letters represent significant differences ($p < 0.05$).

Fig. 2. FE-SEM images of PTS-zein nanoparticles (A), PTS-zein/FU (10:1) nanoparticles (B), PTS-zein/FU (2:1) nanoparticles (C), and PTS-zein/FU (1:2) nanoparticles (D).

Fig. 3. Fluorescence emission spectra of pure PTS in ethanol, zein nanoparticles, PTS-zein nanoparticles, and PTS-zein/FU nanoparticles with different mass ratios of zein to FU.

Fig. 4. FTIR spectra of individual ingredients (PTS, zein, and FU) (A), PTS-zein nanoparticles, and PTS-zein/FU nanoparticles with different mass ratios of zein to FU (B).

Fig. 5. XRD spectra of individual ingredients (PTS, zein, and FU), PTS-zein nanoparticles and PTS-zein/FU nanoparticles with different mass ratios of zein to FU.

Fig. 6. Physical stability of PTS-zein/FU nanoparticles with different mass ratios of zein to FU. The different letters represent significant differences ($p < 0.05$).

Fig. 7. Photochemical stability of PTS in zein nanoparticles, zein/FU (2:1) nanoparticles, and acetonitrile (as control) against UV light. The different letters represent significant differences ($p < 0.05$).

Fig. 8. *In vitro* release profiles of PTS from zein nanoparticles and zein/FU (2:1) nanoparticles in simulated gastrointestinal fluid.

Fig. 9. Cell viability of Caco-2, L-02, and HK-2 cells against zein/FU (2:1) nanoparticles with different concentrations. The different letters represent significant differences ($p < 0.05$).

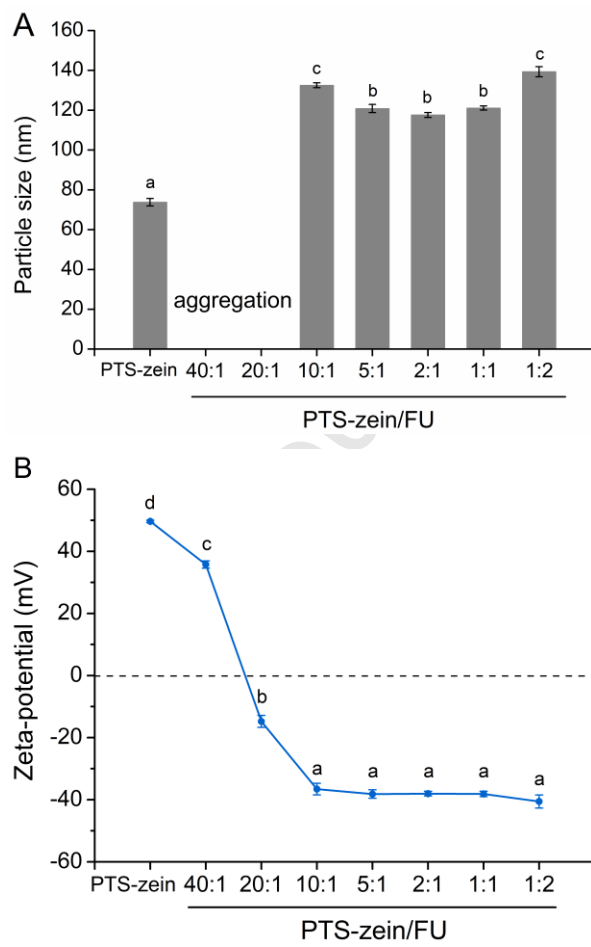
Fig. 10. Schematic illustration of the formation mechanism of PTS-loaded zein/FU composite nanoparticles.

Table 1. Encapsulation efficiency (EE) and loading capacity (LC) of PTS in zein and zein/FU composite nanoparticles ^a

Sample	EE (%)	LC (%)
PTS-zein	86.11 ± 2.95 ^d	7.93 ± 0.25 ^E
PTS-zein/FU (40:1)	47.27 ± 2.78 ^b	4.41 ± 0.25 ^B
PTS-zein/FU (20:1)	27.63 ± 2.27 ^a	2.56 ± 0.20 ^A
PTS-zein/FU (10:1)	92.34 ± 4.90 ^e	7.74 ± 0.38 ^{DE}
PTS-zein/FU (5:1)	95.31 ± 2.53 ^e	7.36 ± 0.18 ^D
PTS-zein/FU (2:1)	95.63 ± 3.86 ^e	5.99 ± 0.23 ^C
PTS-zein/FU (1:1)	89.98 ± 1.57 ^{de}	4.30 ± 0.07 ^B
PTS-zein/FU (1:2)	80.08 ± 2.74 ^c	2.59 ± 0.09 ^A

^a Values were expressed as means ± standard deviation (n = 3). Different lower-case letters (a-e) values represent significant differences ($p < 0.05$) between different EE values of PTS. Different capital letters (A-E) represent significant differences ($p < 0.05$) between different LC values of PTS.

Fig. 1



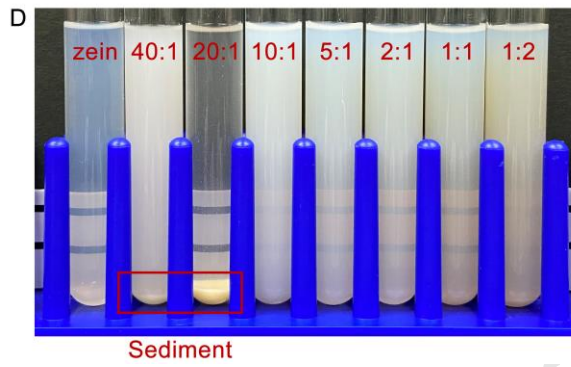
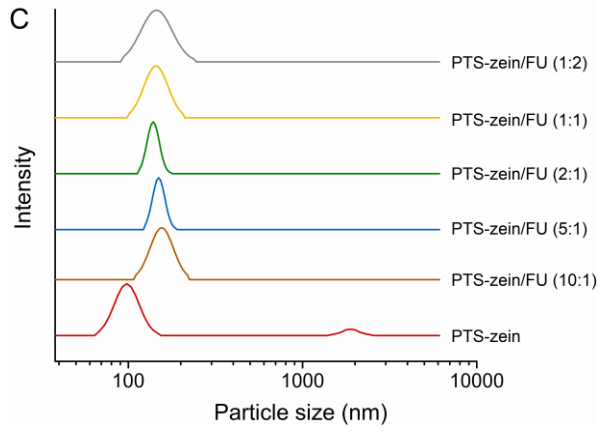


Fig. 2

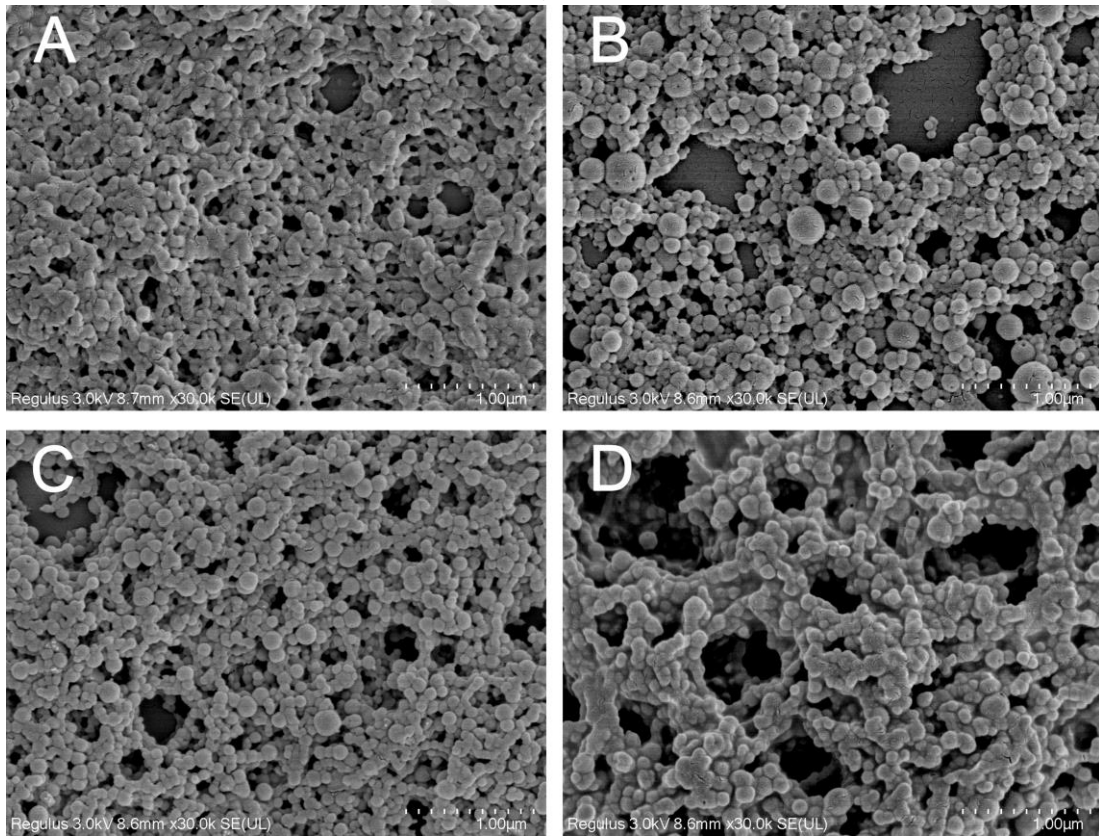


Fig. 3

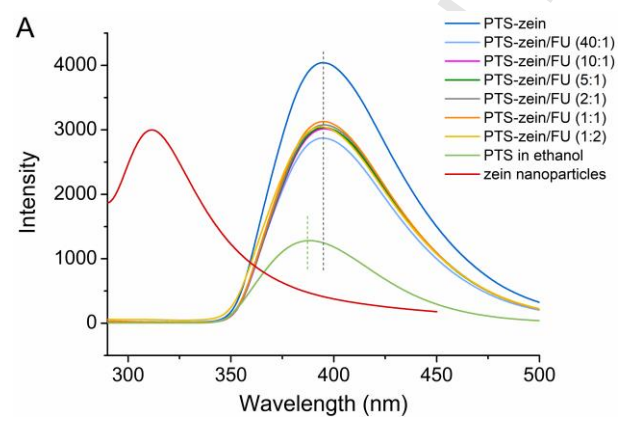
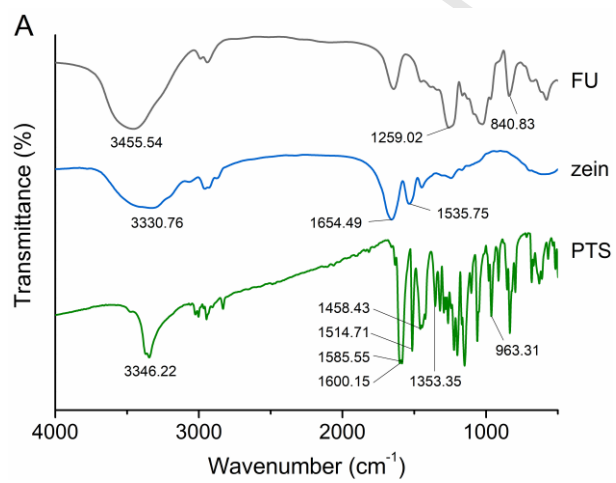


Fig. 4



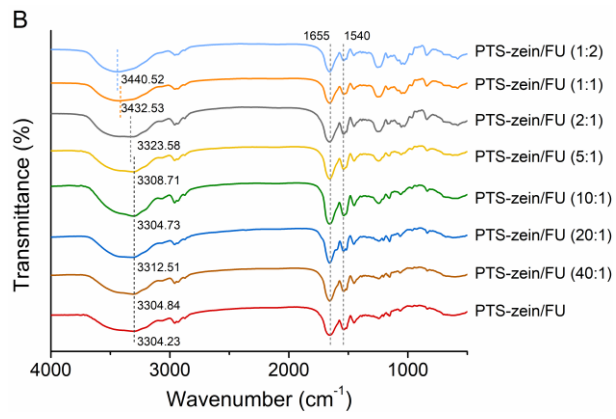


Fig. 5

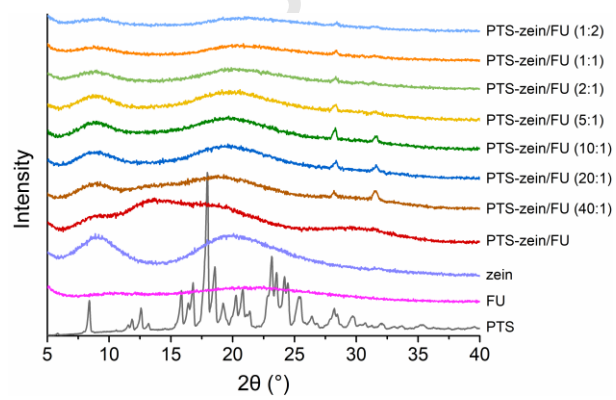


Fig. 6

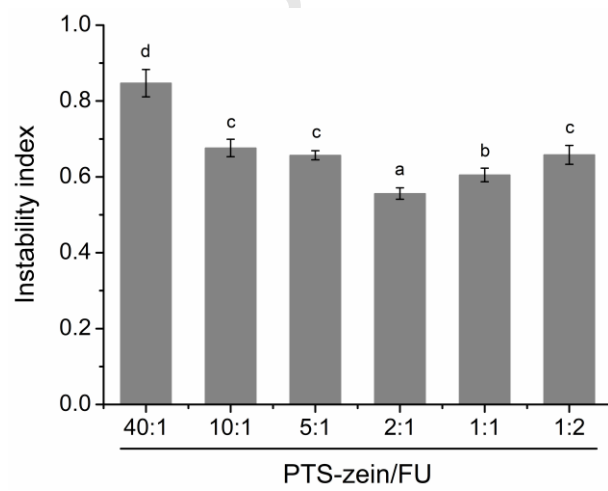


Fig. 7

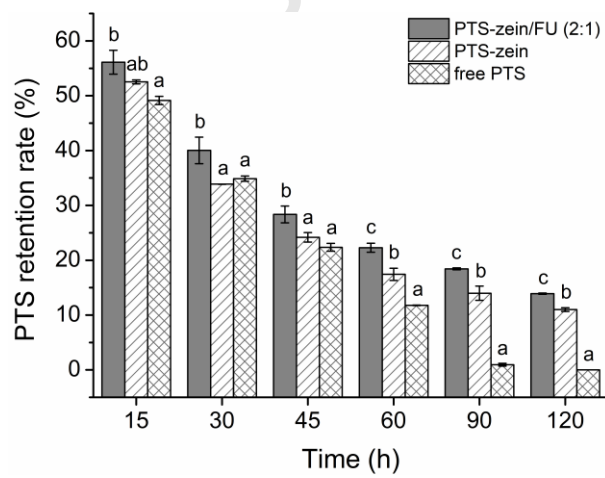


Fig. 8

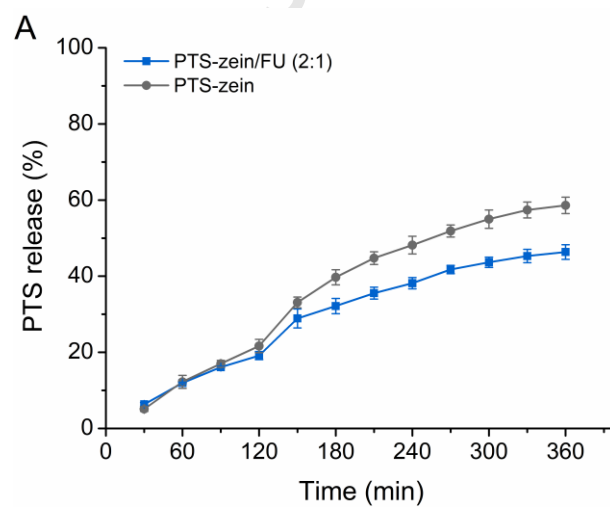
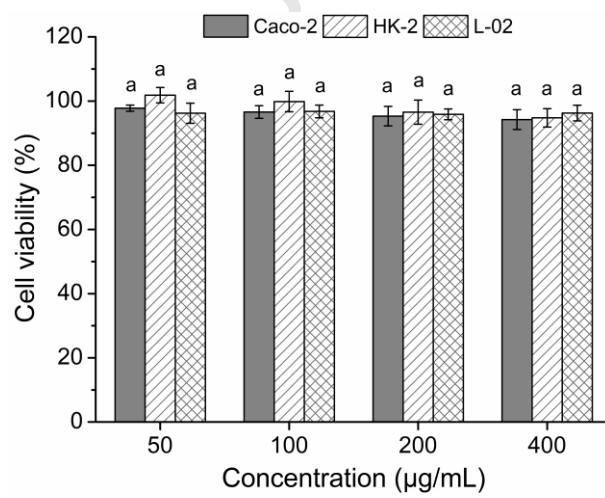


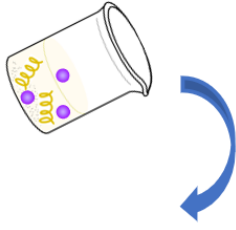
Fig. 9



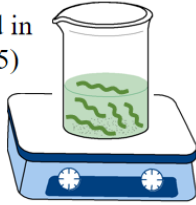
Journal Pre-proof

Fig. 10

zein and PTS dissolved in 75% aqueous ethanol

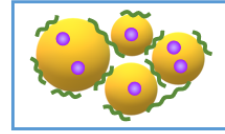


FU dissolved in water (pH 3.5)

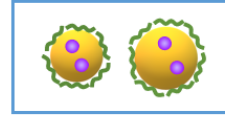


anti-solvent precipitation

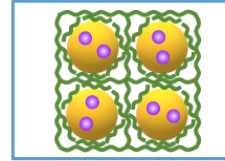
zein/FU mass ratios at 40:1 and 20:1



zein/FU mass ratios at 10:1, 5:1 and 2:1



zein/FU mass ratios at 1:1 and 1:2



zein molecule



FU



PTS



zein nanoparticle



Journal Pre-proof

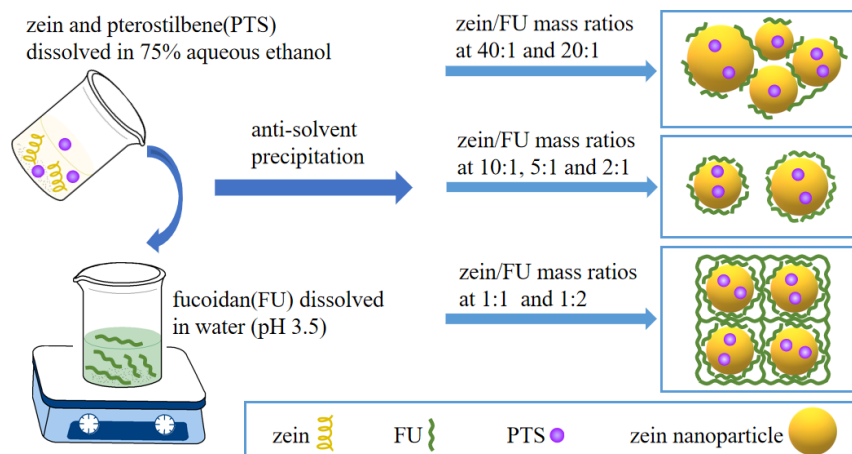
CRedit authorship contribution statement

Qianyuan Liu: Conceptualization, Methodology, Software, Writing - original draft, Data curation.

Jingjing Chen: Formal analysis, Investigation. **Yang Qin:** Software. **Tao Zhang:** Formal analysis, Investigation. **Bo Jiang:** Project administration, Funding acquisition, Writing - review & editing.

Journal Pre-proof

Graphical Abstract



Highlights

- Fucoidan was first used to stabilize zein nanoparticles mainly by electrostatic, hydrogen-bonding, and hydrophobic interactions.
- Zein/fucoidan composite nanoparticles were prepared as a carrier for the delivery of pterostilbene.
- Zein to fucoidan mass ratios influenced the physicochemical properties of composite nanoparticles.
- The addition of fucoidan into composite nanoparticles improved the encapsulation efficiency and photochemical stability of pterostilbene.
- Zein/fucoidan nanoparticles exhibited a controlled release of pterostilbene and no cytotoxicity.